metals

MDPI

Article

Effect of Slag Chemistry on the Smelting Reduction Behavior of Chromite Ore

Yijian Zhang [1], Jianliang Zhang [1,*], Ping Du [2], Yu Lu [2], Xun Zhou [1], Miao Luo [1] and Jianyang Yin [1]

[1] School of Metallurgical and Ecological Engineering, University of Science and Technology Beijing, Beijing 100083, China; zhangyijian0727@163.com (Y.Z.)
[2] Institute of Research of Iron & Steel, Shagang, Zhangjiagang 215625, China
* Correspondence: zhang.jianliang@hotmail.com

Abstract

This study aims to investigate the effects of slag chemical composition on the smelting reduction behavior and microstructural evolution of chromite at 1525–1550 °C, thereby providing theoretical guidance for optimizing the smelting reduction process. Through high-temperature melting experiments combined with Scanning Electron Microscope - Energy Dispersive Spectrometer(SEM-EDS) microstructural characterization and thermodynamic calculations, the influences of basicity, MgO content, and Al_2O_3 content on chromium reduction behavior, slag physicochemical properties, and spinel evolution mechanisms were systematically analyzed. The results indicate that a basicity of 1.2 effectively promotes the dissolution and reduction of chromium spinel, whereas excessively high basicity hinders the reduction process when using graphite as the reducing agent. Although increasing MgO content initially improves slag fluidity and reaction rates, it promotes the formation of a Mg-Al-rich solid product layer during the later stages of the reaction; this restricts the intra-phase diffusion of Cr^{3+} and causes the reduction process to stall. High Al_2O_3 content significantly increases system viscosity and impairs mass transfer, thereby reducing the degree of reduction. Under optimized conditions, specifically an Al_2O_3 content of 14 wt% and a temperature of 1550°C, the degree of reduction approaches 93%. Thermodynamic calculations further reveal that the efficiency of chromite smelting reduction is synergistically controlled by factors such as slag viscosity, liquid-phase behavior, and spinel equilibrium phase mass. The favorable slag composition identified in this study, basicity of 1.2, MgO content of 10 wt%, and Al_2O_3 content of 14 wt%, provides favorable physicochemical conditions for the efficient smelting reduction of chromite.

Keywords: smelting reduction; chromite ore; slag properties; microstructural evolution

Check for updates

Academic Editor: Mark E. Schlesinger

Received: 30 June 2026
Revised: 2 August 2026
Accepted: 6 August 2026
Published: 10 August 2026

Copyright: © 2026 by the authors. Licensee MDPI, Basel, Switzerland. This article is an open access article distributed under the terms and conditions of the Creative Commons Attribution (CC BY) license.

1. Introduction

In pyrometallurgical processes, slag serves as the fundamental medium for heat transfer, mass transfer, and interfacial chemical reactions; for the smelting reduction of chromite, the physicochemical properties of the slag determine the efficiency of the entire process. Due to the high stability of the chromium-bearing spinel structure, and unlike conventional submerged-arc furnace smelting, intense-stirring smelting reduction processes (such as HIsmelt) drive reactions at the slag–metal interface through continuous gas injection; the rapid dissolution and mass transfer of chromium spinel within the slag significantly accelerate this process [1–5]. Therefore, optimizing slag fluidity and thermodynamic properties is a crucial approach to enhancing chromium recovery and accelerating smelting efficiency [6–8].

Variations in slag composition can significantly alter slag viscosity, liquidus temperature, and structural polymerization characteristics, thereby influencing component diffusion and reaction behavior at the slag–metal interface [9–13]. In particular, the migration, crystallization, and reduction behaviors of chromium oxides are closely linked to the structural stability and evolution of high-temperature slag. Chen et al. [14] indicated that increasing Al_2O_3 and Cr_2O_3 contents promotes the polymerization of the silicate network, thereby raising slag viscosity and inducing the premature precipitation of complex spinel phases, such as high-melting-point $MgCr_2O_4$, which affects slag mass transfer behavior. The addition of an appropriate amount of FeO can effectively lower the slag liquidus temperature and system viscosity, thereby improving overall fluidity [15]. Furthermore, high basicity and low oxygen potential environments promote the migration of chromium from the liquid slag into the solid-phase crystal lattice, leading to the stable precipitation of spinel phases that form a solid-product layer hindering reduction [16,17]. Regarding micro-kinetics and interfacial mass transfer, T. Nakasuga [18] and O. Demir et al. [19] pointed out that the reduction and dissolution processes of chromite particles in slag are controlled by ion mass transfer at the solid–liquid interface, including the diffusion of oxygen ions within the boundary layer. Consequently, in high-temperature molten systems utilizing carbonaceous reducing agents, changes in slag chemical composition not only directly determine the chromite dissolution rate and mass transfer kinetics but also accelerate the evolution of the solid-product layer at the microscopic interface, thereby influencing the overall reduction process [20–22]. Although previous studies have clearly elucidated the phase evolution and mass transfer mechanisms in traditional carbon-bed smelting, the dominant factors often vary depending on slag composition and reaction conditions—particularly under the intense gas stirring characteristic of the molten bath. Therefore, further in-depth investigation is required to understand the specific reaction behavior under the conditions of the smelting reduction process.

To optimize the slagging practice and ensure efficient chromium extraction, this study investigates the effect of slag composition on the smelting reduction efficiency of chromite. By integrating physicochemical property analysis with microstructural characterization, the study explores the relationships among slag chemical composition, mass transfer behavior, and the chromite reduction mechanism, thereby providing theoretical guidance for the efficient smelting reduction of chromite.

2. Materials and Methods

2.1. Melt Reduction Experiment

This experiment aims to reveal the effect of slag composition on the smelting reduction reaction of chromite. The experiments were conducted using a high-temperature tube furnace manufactured by Boleimante (BLMT-1700, Luoyang, China), with a maximum operating temperature of up to 1700 °C. A schematic diagram of its structure is shown in Figure 1. The furnace consists of silicon molybdenum heating elements, an alumina tube, refractory bricks, and a thermocouple. The thermocouple is a Type B platinum-rhodium thermocouple, and the thermocouple is placed in close contact with the constant-temperature zone. The electrical control cabinet features a built-in intelligent heating system regulated by Proportional-Integral-Derivative (PID) control, maintaining temperature precision within 1 °C. A mixed gas of N_2 + CO + CO_2 was used to simulate the atmosphere of the smelting reduction process. The gases were stored in a gas cylinder cabinet, delivered to the gas transmission pipeline built into the electrical control cabinet through a gas mixing tank, and finally introduced into the furnace from the bottom.

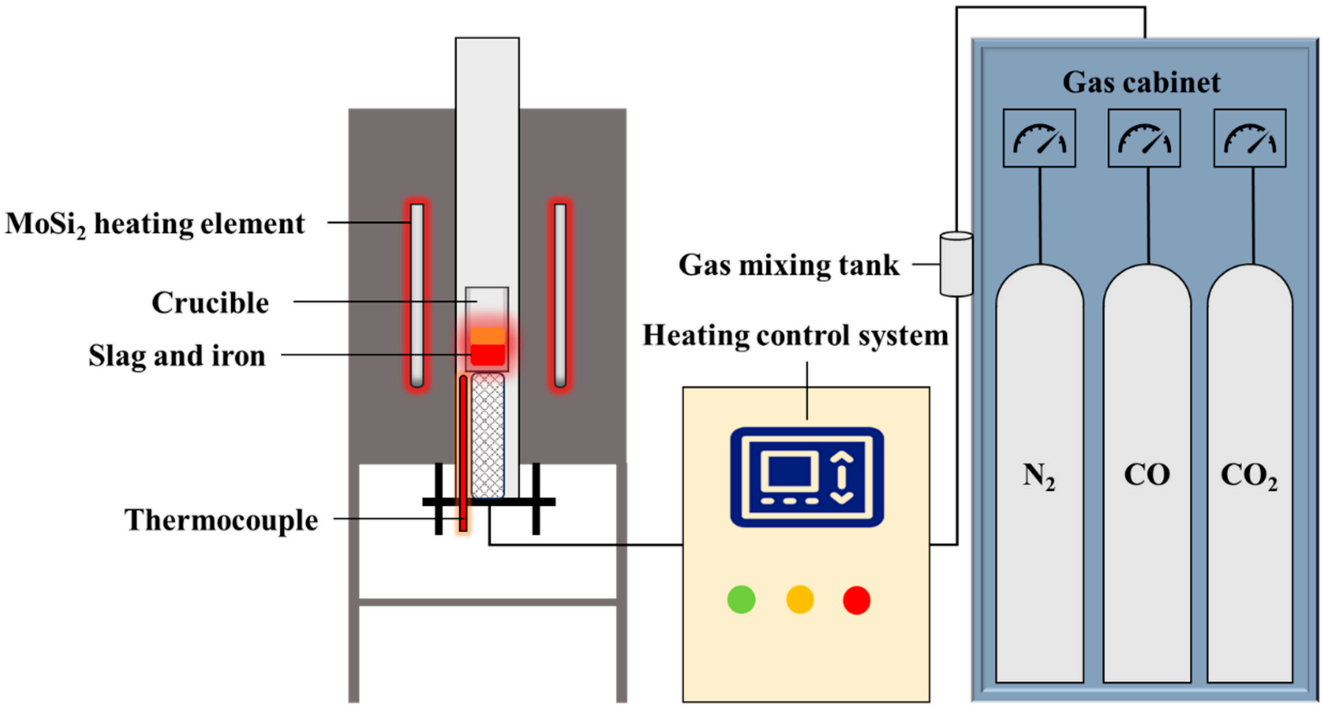


Figure 1. Schematic diagram of the structure of the high-temperature tube furnace.

The experiment used chemically pure reagents including iron powder, graphite powder, and silicon powder (Macklin, Shanghai, China, purity > 99%) to prepare 200 g of the initial molten iron. Analytical-grade oxide reagents including CaO, SiO_2, MgO, and Al_2O_3 (Macklin, purity > 99%) were used as slag-forming agents. Based on industrial practice, the slag-to-iron ratio was set at 0.3, and the slag mass in the experiment was 66.51 g. Twenty grams of chromite powder was used as the reactant, and additional graphite (Macklin, Shanghai, China, purity > 99.95%, 850 mesh) was added as the reducing agent. The amount of graphite added was calculated based on a C/O ratio of 1.2, and the added amount is 8.69 g. The composition of the chromite is shown in Table 1. A laser particle size analyzer (Mastersizer 3000, Malvern Panalytical, Malvern, UK), with a measurement range of 0.01–3500 μm, was used to determine the particle size distribution of the chromite ore. As shown in Figure 2, the particle size of the chromite ore powder primarily falls within the 40–900 μm range; the 76–186 μm interval constitutes the main concentration zone, accounting for 59.23% of the total. Particles larger than 76 μm make up 83.66% of the total, thereby meeting the particle size requirements for ore powder injection in the smelting reduction process.

Table 1. Chemical Composition of Chromite Powder (wt%).

TFe	FeO	Fe_2O_3	Cr_2O_3	CaO	SiO_2	MgO	Al_2O_3
21.88	4.37	26.40	43.30	0.09	1.77	8.93	13.00
TiO_2	**V_2O_5**	**MnO**	**Na_2O**	**ZnO**	**K_2O**	**P**	**S**
0.61	0.38	0.20	0.01	<0.01	<0.01	<0.01	0.01

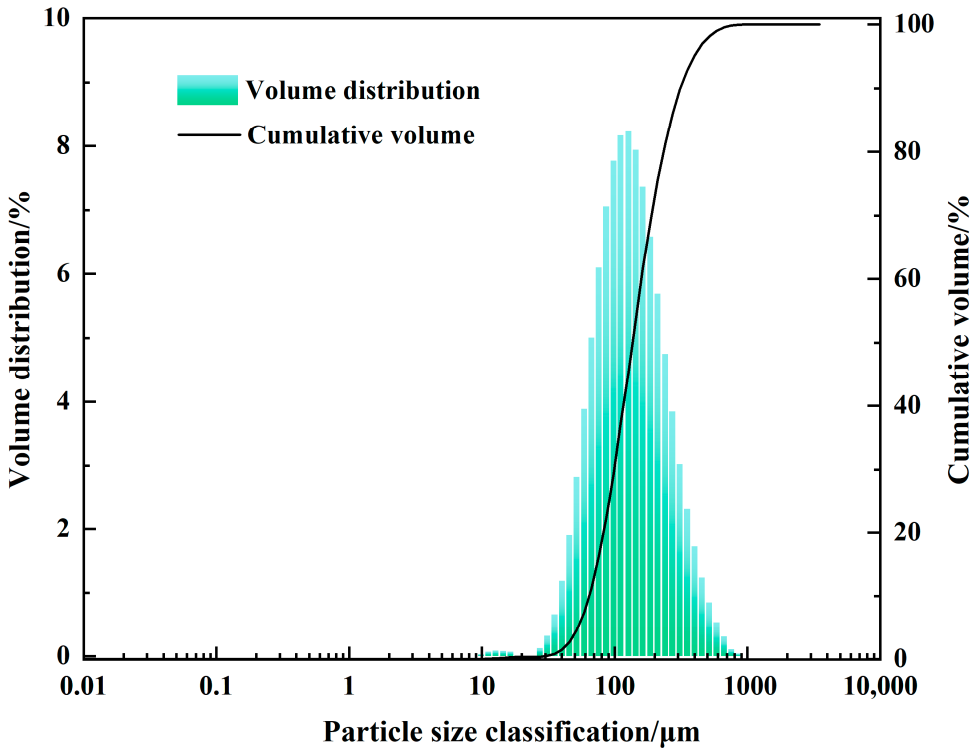


Figure 2. Particle size distribution of chromite powder.

Before the experiment, all reagents were dried and dehumidified and then ground in an agate mortar to ensure homogeneous mixing. First, the hot metal powder sample was placed into a corundum crucible with an inner diameter of 5.5 cm and a height of 10 cm, with an additional outer corundum crucible used as a protective crucible. The reaction time was limited to 120 min, and the slag quantity was controlled to minimize potential crucible dissolution; the crucible did not significantly obscure the expected compositional gradient within the bulk slag. Consequently, the impact of corundum crucible dissolution on the overall slag composition was considered negligible. The crucible was positioned within the constant-temperature zone of a tube furnace. High-purity nitrogen was introduced at a flow rate of 2.5 L/min, after which the heating program was initiated to begin the melting process. Once the furnace temperature reached the target value, it was maintained for 30 min to ensure compositional homogeneity of the molten iron bath. The prepared reaction mixture (chromite powder, slag-forming agent, and reducing agent) was then added into the crucible containing the iron bath through a corundum tube with an inner diameter of 3 cm and a length of 80 cm. Natural convection and density-driven circulation promoted mixing of the molten bath. The moment of high-temperature addition was recorded as the reaction start time, t_0 = 0 min. In the smelting reduction process, oxygen-enriched hot air is injected into the upper part of the furnace, resulting in an internal atmosphere composed of N_2, CO, and CO_2; therefore, the gas used in this experiment was switched to an N_2-CO-CO_2 mixture with a CO_2-to-CO ratio of 1:1. The flow rates were 2.5 L/min for N_2, 1.25 L/min for CO, and 1.25 L/min for CO_2. At t = 15, 30, 45, 60, 90, and 120 min, a quartz tube with a diameter of 8 mm was inserted approximately 1–2 cm into the molten iron. Molten iron was withdrawn by negative-pressure suction and immediately water-quenched for subsequent compositional analysis. Approximately 10 g of molten metal was withdrawn at each sampling interval. The chromium content in the quenched metal samples was quantitatively analyzed using Inductively Coupled Plasma Optical Emission Spectrometry (ICP-OES). The instrument used was an Agilent 5110 (Santa Clara, CA, USA), sample pretreatment involved microwave digestion, with a final volume of 25 mL and

a dilution factor of 10. Each sample was measured in triplicate, and the average value was calculated. The microstructural evolution and elemental distribution of the reacted slag were characterized using a Scanning Electron Microscope (SEM, Zeiss Gemini Sigma 300 VP, Oberkochen, Germany) equipped with an Energy Dispersive Spectrometer. Prior to observation, the quenched slag samples were embedded in epoxy resin, progressively ground using abrasive papers. To ensure sufficient electrical conductivity during imaging, a thin layer of gold was coated onto the polished sample surfaces. As the analyses focused on spatial elemental distribution and phase boundary morphology, the EDS data were collected primarily in qualitative mapping mode. The detailed experimental scheme and the composition of the initial molten iron are presented in Table 2. The slag basicity (R) was defined as the mass ratio of CaO to SiO_2.

$$\mathrm{R} = \frac{wt\%CaO}{wt\%SiO_2} \tag{1}$$

where wt%CaO and wt%SiO_2 represent the mass fractions of CaO and SiO_2 in the slag, respectively.

Table 2. Melting reduction experiment scheme (wt%).

No	Composition of Slag					Composition of Molten Iron			Temperature
	CaO	SiO_2	MgO	Al_2O_3	Basicity	Fe	C	Si	
1	37.00	37.00	10	16	1.0	95.7	4.0	0.3	1525
2	40.36	33.64	10	16	1.2	95.7	4.0	0.3	1525
3	43.17	30.83	10	16	1.4	95.7	4.0	0.3	1525
4	41.45	34.55	8	16	1.2	95.7	4.0	0.3	1525
5	39.27	32.73	12	16	1.2	95.7	4.0	0.3	1525
6	41.45	34.55	10	14	1.2	95.7	4.0	0.3	1525
7	39.27	32.73	10	18	1.2	95.7	4.0	0.3	1525
8	41.45	34.55	10	14	1.2	95.7	4.0	0.3	1550

In addition, this paper defines the reduction degree of chromite, calculated based on the ratio of the Cr mass in samples taken at different times to the Cr mass originally introduced by the ore, as shown in Equation (2). The reaction rate was determined by calculating the derivative of the chromium concentration with respect to time between discrete sampling points, expressed as Equation (3). The experimental data points were connected using B-spline interpolation to guide visualization of the changing trends. No additional data points were generated, and the interpolation did not affect the original experimental values.

$$\text{Degree of Reduction } (\%) = \frac{m_{metal} \times [\%Cr]_{metal}}{m_{chromite} \times [\%Cr]_{chromite}} \times 100\% \tag{2}$$

$$\text{Reaction rate } \left(\text{min}^{-1}\right) = \frac{\Delta[\%Cr]}{\Delta t} \tag{3}$$

2.2. Thermodynamic Calculations of Slag Properties

To further elucidate the influence of slag composition on the smelting reduction behavior of chromite, thermodynamic calculations and viscosity modeling were combined to analyze the physicochemical properties of the slag. The slag viscosity was calculated using the modified Urbain model [23–25], which is widely applied to metallurgical slags in the CaO-SiO_2-MgO-Al_2O_3 system. Based on the Weymann–Frenkel equation, this model correlates the high-temperature viscosity of slags with absolute temperature and the microscopic

structural parameters of the melt. By classifying oxide components in the slag into network formers, network modifiers, and amphoteric oxides, thermodynamic parameters reflecting the degree of structural polymerization and the viscous flow activation energy can be determined, enabling relatively accurate prediction of high-temperature slag viscosity.

$$\eta = ATexp\left(\frac{B}{T}\right) \tag{4}$$

where η represents dynamic viscosity (Pa·s), T represents absolute temperature (K), A represents the pre-exponential coefficient, and B represents the temperature-dependent parameter (K). The parameters A and B are composition-dependent and are determined from the normalized slag composition according to the modified Urbain model.

$$-lnA = a + bB \tag{5}$$

where a and b are empirical constants defined in the modified Urbain model. The parameter B is calculated as a polynomial function of the normalized oxide composition:

$$B = f(X_i) \tag{6}$$

In this work, the viscosities of slags with different compositions were predicted in the temperature range of 1400–1600 °C. Considering the atmospheric conditions during the smelting reduction process, the FeO and Cr_2O_3 contents in the slag were fixed at 4 wt% and 1 wt%, respectively, in the calculations in order to evaluate the effects of slag composition on fluidity and mass transfer behavior. The calculated viscosity represents the intrinsic viscosity of the liquid slag phase and does not include the effect of suspended solid particles. For heterogeneous suspension systems containing solid spinel, the apparent viscosity will inevitably be higher. The theoretical liquid phase content at the experimental temperature is above 98%; therefore, the calculation results of the Urbain model can be used as a benchmark for measuring flowability.

Meanwhile, thermodynamic simulations were performed using the Equilib module of FactSage (Version 8.3) to calculate the liquidus temperature and liquid fraction of the CaO-SiO_2-Al_2O_3-MgO-FeO-Cr_2O_3 slag system under equilibrium conditions. The FactPS and FToxid databases were selected for the calculations. The total amount of slag is calculated based on 100 g. The slag composition range was kept consistent with that used in the viscosity calculations. The basicity was set in the range of 1.0–1.4, MgO content from 8 to 12 wt%, and Al_2O_3 content from 14 to 18 wt%, with the temperature range set from 1000 to 1600 °C at 50 °C intervals. The pressure is 1 atm, all solution phases are selected, and Slag-Liq is set as the target phase. In addition, to further investigate the reduction mechanism of chromite, the equilibrium contents of $MgCr_2O_4$, $FeCr_2O_4$, and $MgAl_2O_4$ spinel phases as a function of temperature were calculated to evaluate the stability and dissolution behavior of spinel phases under different slag compositions. Combined with experimental results and SEM analysis, the influence of slag composition on the dissolution and reduction kinetics of chromite was elucidated.

3. Results and Discussion

3.1. Effect of Slag Composition on Reduction Behavior

Changes in slag phase composition directly affect mass transfer and diffusion processes within the phase; therefore, it is necessary to investigate the reduction behavior under different compositions. Figure 3a shows the variation in Cr content in hot metal under different basicities. It can be seen that as the basicity increases from 1.0 to 1.4, the Cr content

first increases and then decreases. When the basicity is 1.0, the slag exhibits insufficient fluidity and the liquid-phase mass transfer process is hindered; thus, the final Cr content is only 0.95 wt%. When the basicity increases to 1.2, the Cr content reaches 2.31 wt%, while further increasing the basicity to 1.4 leads to a decrease in the final Cr content to 1.18 wt%.

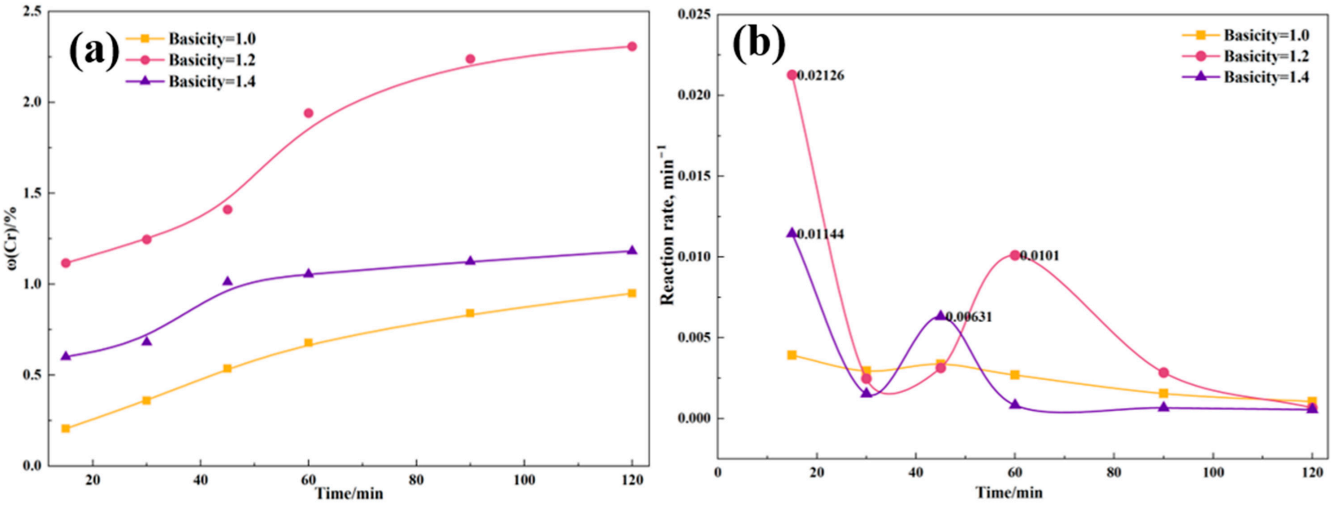


Figure 3. Cr content and reaction rate at different basicities at 1525 °C. (**a**) Cr content, wt%; (**b**) Reaction rate, min^{-1}.

The reaction conversion rates at different basicities are shown in Figure 3b. When the basicity is 1.0, the conversion rate remains very low throughout the entire reaction period, with a maximum value of only 0.0039 min^{-1}. As the basicity increases to 1.2, the conversion rate increases significantly. At the initial stage of the reaction, the maximum conversion rate reaches 0.0213 min^{-1}. In addition, at around 60 min, a peak appears in the reaction rate curve, with a value of 0.0101 min^{-1}. Previous studies [2,19,26] have indicated that the reduction of chromite is a multi-stage rate-controlled process: the early stage is inferred to be governed interfacial boundary layer reactions, while the later stage is governed intra-phase diffusion. The change in reaction rate at 60 min is attributed to the transition of the rate-controlling step. When the basicity is 1.4, the initial reaction rate is 0.0114 min^{-1}, and the time required to reach the peak rate is shortened from 60 min to 45 min; thereafter, the reaction rate decreases to 0.0063 min^{-1}.

The variations in Cr content and reaction rate at different MgO contents are shown in Figure 4. As the MgO content increases from 8 wt% to 12 wt%, the final Cr contents are 2.23 wt%, 2.31 wt%, and 2.24 wt%, respectively. Benefiting from improved mass transfer conditions, the conversion rate increases from 0.0150 min^{-1} to 0.0213 min^{-1}. When the MgO content is 12 wt%, the initial Cr content is relatively low at 0.56 wt%, and the initial reaction rate is only 0.0106 min^{-1}. At 30 min, the reaction rate reaches 0.0210 min^{-1}. With further extension of time, the Cr content becomes nearly stagnant after 60 min. In the later stage, the process is inferred to be governed intra-phase diffusion. The magnesium aluminate spinel product layer surrounding the chromite spinel becomes thicker, which hinders diffusion. Therefore, the reaction rate at 60 min decreases with increasing MgO content from 0.0160 min^{-1} to 0.0041 min^{-1}.

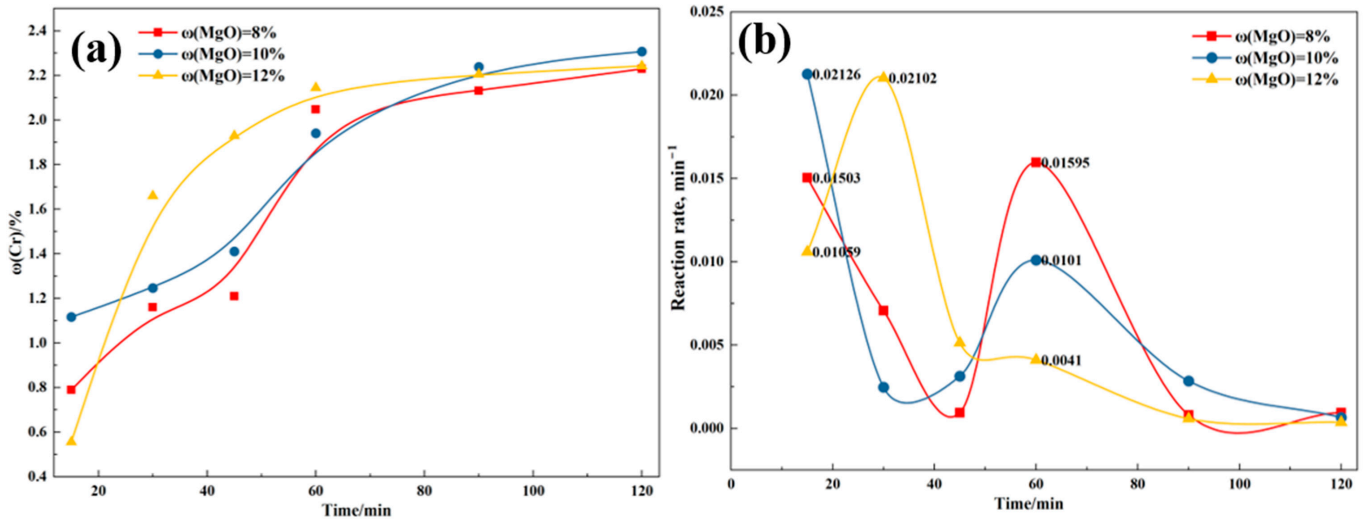


Figure 4. Cr content and reaction rate at different MgO contents at 1525 °C. (**a**) Cr content, wt%; (**b**) Reaction rate, min^{-1}.

Figure 5a shows the variation in Cr content under different Al_2O_3 conditions. As the Al_2O_3 content increases from 14 wt% to 18 wt%, the final Cr content decreases from 3.05 wt% to 2.23 wt%, indicating that high-alumina conditions weaken slag fluidity and hinder mass transfer and diffusion processes, thereby exerting a negative effect on the smelting reduction of chromite. In addition, this section further investigates the Cr content evolution at 1550 °C when the Al_2O_3 content is 14%. It can be seen that increasing the temperature to 1550 °C significantly promotes the reduction reaction, resulting in a final Cr content of 3.23 wt%, corresponding to a chromite reduction degree close to 93%. The reaction rates at different Al_2O_3 contents are shown in Figure 5b. When the Al_2O_3 content is 16 wt% and 18 wt%, the initial conversion rates are 0.0213 min^{-1} and 0.0193 min^{-1}, respectively, which are higher than that at 14 wt% Al_2O_3, possibly due to the rapid dissolution of chromite spinel. In addition, when the temperature increases to 1550 °C, the conversion rate at 14 wt% Al_2O_3 increases from 0.0091 min^{-1} to 0.0144 min^{-1}. With increasing reaction time, the later stage where diffusion resistance becomes increasingly important. Moreover, the higher alumina slag exhibits higher viscosity and deteriorated fluidity, leading to the formation of a solid product layer around chromite spinel, which further reduces the reaction rate.

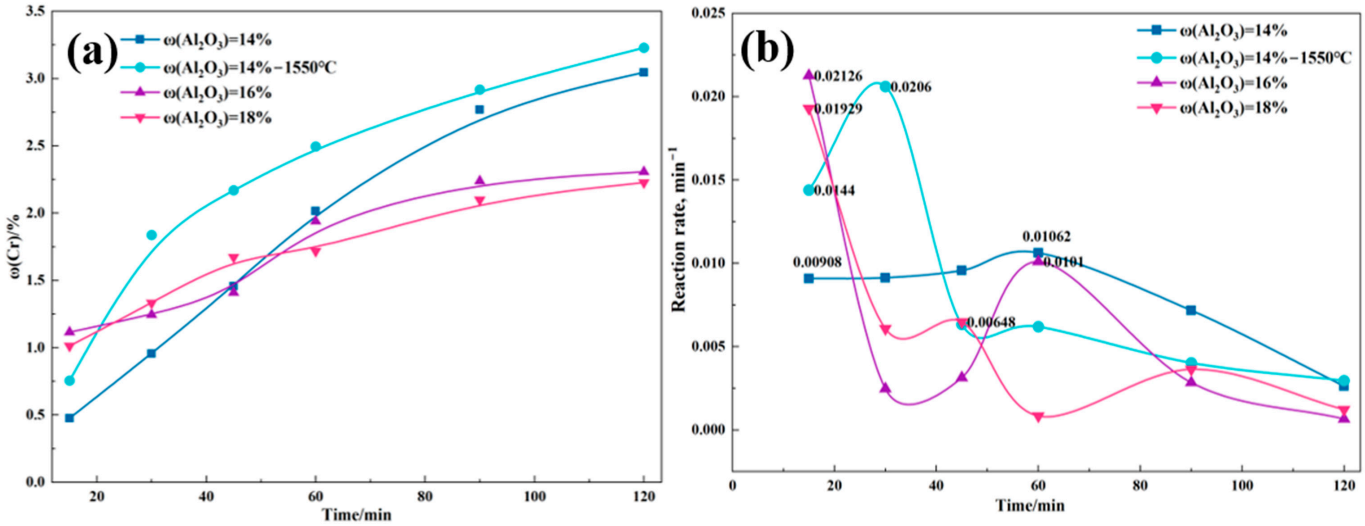


Figure 5. Cr content and reaction rate at different Al_2O_3 contents. (**a**) Cr content, wt%; (**b**) Reaction rate, min^{-1}.

To more clearly demonstrate the effect of slag composition on chromite reduction, Table 3 lists the reduction degrees at different times. It can be seen that the degree of reduction improved significantly with changes in basicity; furthermore, at 1550 °C (No. 8), the reduction degree approached 93%.

Table 3. Degree of reduction under different conditions (%).

No	Degree of Reduction/%						Temperature/°C
	15 min	30 min	45 min	60 min	90 min	120 min	
1	5.86	10.27	15.31	19.35	23.97	27.10	1525
2	31.89	35.60	40.29	55.44	63.95	65.91	1525
3	17.16	19.45	28.91	30.15	32.13	33.77	1525
4	22.55	33.15	34.56	58.48	60.89	63.70	1525
5	15.89	47.42	55.12	61.27	63.00	64.07	1525
6	13.63	27.32	41.67	57.60	79.11	87.02	1525
7	28.94	38.07	47.79	49.05	59.96	63.63	1525
8	21.60	52.50	62.00	71.29	83.36	92.24	1550

3.2. Analysis of Microstructural Evolution and Interface Characteristics

As shown in Figure 6, the SEM characterization results under different basicity conditions indicate that the gray regions in Figure 6a–f correspond to the slag matrix, while the white blocky particles represent unreacted chromite spinel. When the basicity is 1.0 and 1.4, the chromite spinel particles are relatively large with sharp edges and clear outlines. In contrast, when the basicity is 1.2, the particle size of chromite spinel decreases and the edges become blurred, showing a transitional state with the slag matrix and gradually forming a liquid reaction layer. While these two-dimensional cross-sectional observations are strictly qualitative, this morphological evolution, regarding particle rounding and size reduction, visually corroborates the macroscopic kinetic results, illustrating the enhanced dissolution behavior of the chromium spinel.

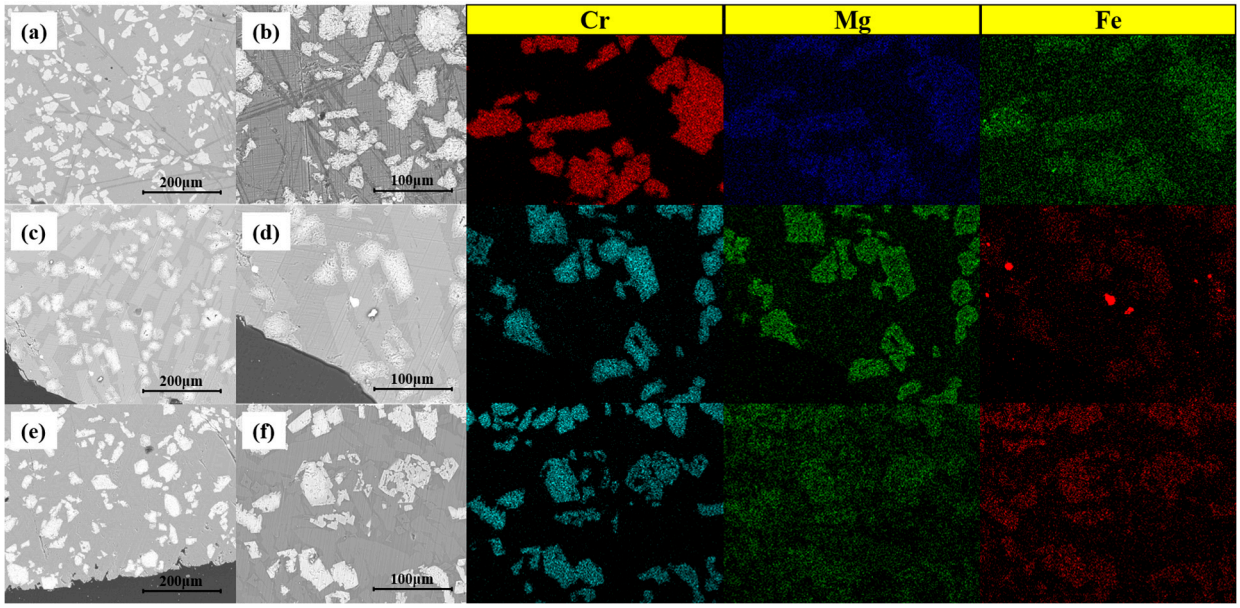


Figure 6. SEM analysis at different basicities: (**a**) Basicity=1.0 sample, 200 μm. (**b**) Basicity=1.0 sample, 100 μm. (**c**) Basicity=1.2 sample, 200 μm. (**d**) Basicity=1.2 sample, 100 μm. (**e**) Basicity=1.4 sample, 200 μm. (**f**) Basicity=1.4 sample, 100 μm.

Energy-dispersive spectroscopy (EDS) mapping further reveals that Mg exhibits a progressively more dispersed distribution with increasing basicity. At a basicity of 1.0, Cr and Mg are mainly co-enriched, while Fe is present both in chromite spinel and in the slag

matrix. At a basicity of 1.2, Cr and Mg remain enriched; however, the Fe signal in both the slag matrix and chromite spinel decreases, and metallic iron appears in the form of bright phases in BSE images. When the basicity increases to 1.4, a significant amount of Mg is present in the slag matrix, while Mg enrichment in chromite spinel is weakened, indicating that increasing basicity promotes chromite dissolution. In addition, due to the reduced reaction degree at a basicity of 1.4, Fe remains densely distributed within the unreacted spinel core.

As shown in Figure 7, Cr and Mg still exhibit obvious enrichment behavior under different MgO contents. EDS mapping shows that Al is widely distributed in both the slag matrix and the outer layer of chromite spinel, while its content inside the spinel is relatively low. Furthermore, when the MgO content increases to 12 wt%, the enrichment of Mg and Al in the outer layer of chromite spinel becomes more pronounced, indicating that a Mg-Al-rich spinel layer, possibly corresponding to $MgAl_2O_4$, forms around chromite spinel during the reaction. This layer hinders the diffusion of internal Cr ions, thereby slowing the reaction rate, which is consistent with previous studies.

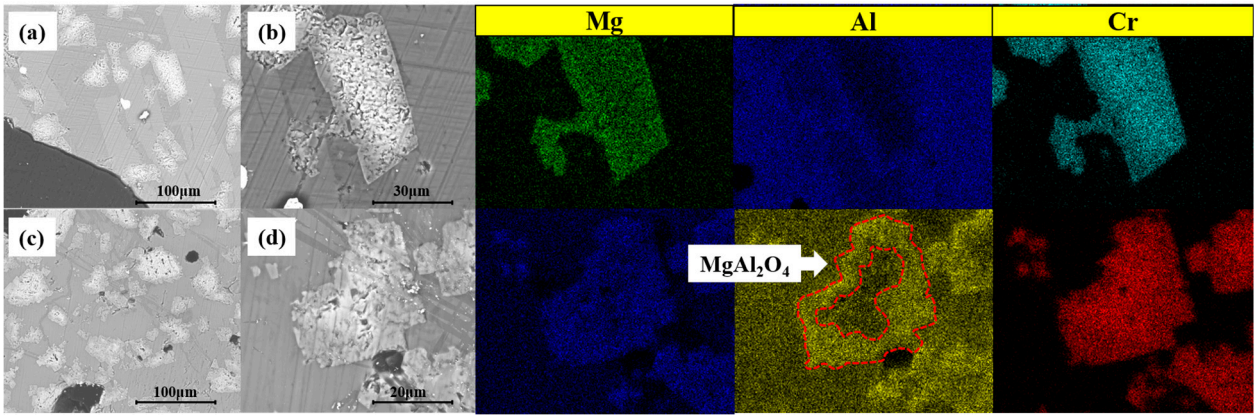


Figure 7. SEM analysis at different MgO contents: (**a**) 10 wt% MgO sample, 200 μm; (**b**) 10 wt% MgO sample, 100 μm; (**c**) 12 wt% MgO sample, 200 μm; (**d**) 12 wt% MgO sample, 100 μm.

SEM observations show that as the Al_2O_3 content increases from 14 wt% to 18 wt%, the number of chromite spinel particles increases significantly (Figure 8c–f), and the enrichment of Fe, Cr, and Mg becomes more pronounced. When the Al_2O_3 content is 14 wt%, the Fe content in chromite spinel decreases and dispersed metallic iron appears in the slag matrix. As discussed above, this condition corresponds to the highest chromite reduction degree. In addition, the upper layer of post-reaction slag samples was also characterized. As shown in Figure 8a,b, large regions of iron oxides were observed in the upper slag layer, and chromite spinel in these regions was also encapsulated by Fe-rich oxide phases. The upper slag corresponds to an incompletely reacted zone, which suggests that during chromite reduction, Fe^{2+} in chromite spinel is reduced prior to Cr^{3+}. As the reaction proceeds, Fe^{2+} in the outer region is continuously consumed, and internal Fe^{2+} migrates outward to sustain the reduction process. Figure 9 illustrates the Gibbs free energy for the reduction of chromite by carbon in molten iron; under standard conditions, the onset reduction temperature of $FeCr_2O_4$ is significantly lower than that of $MgCr_2O_4$. At 1600 °C, the thermodynamic driving force for the reduction of $FeCr_2O_4$ is −54.68 kJ, whereas that for the reduction of $MgCr_2O_4$ is −28.64 kJ. Eric et al. [27–29] also reported that after Fe ions at the chromite surface are reduced to the metallic state, Cr ions diffuse toward the core and replace internal Fe ions. When both Fe and Cr ions are fully reduced, a Mg-Al-rich spinel layer is formed. It should be noted that some phases observed by SEM-EDS may have formed during cooling rather than being stable phases at the experimental temperature.

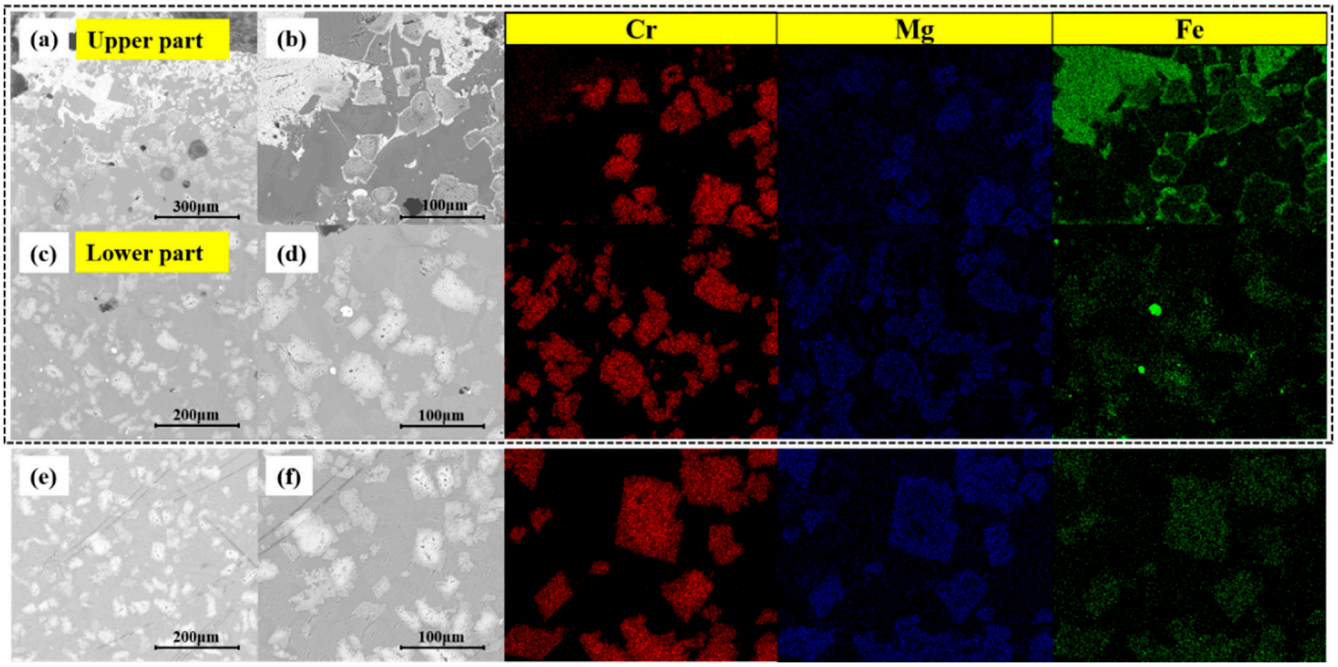


Figure 8. SEM analysis at different Al_2O_3 contents: (**a**) 14 wt% Al_2O_3 sample, upper 200 μm; (**b**) 14 wt% Al_2O_3 sample, upper 100 μm; (**c**) 14 wt% Al_2O_3 sample, lower 200 μm; (**d**) 14 wt% Al_2O_3 sample, lower 100 μm; (**e**) 18 wt% Al_2O_3 sample, 200 μm; (**f**) 18 wt% Al_2O_3 sample, 100 μm.

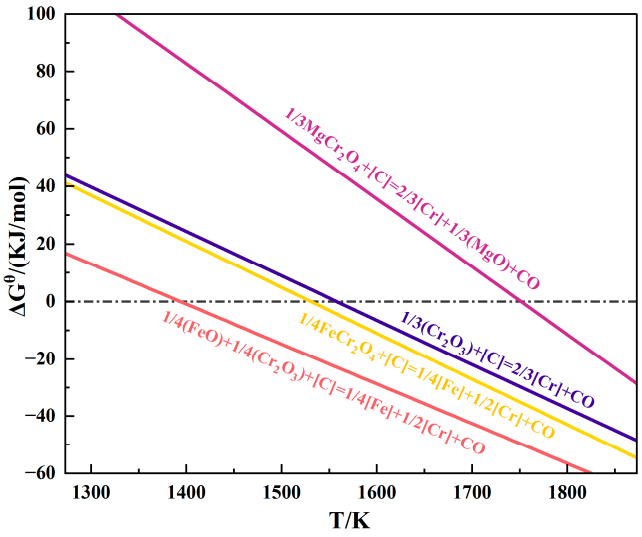


Figure 9. Gibbs free energy of chromite reduced by molten iron [C]. (The dashed line represents the baseline where the standard Gibbs free energy equals zero).

3.3. Slag Physicochemical Properties

As discussed above, changes in slag composition directly affect its fluidity and phase precipitation behavior. Figure 10a–c presents the calculated slag viscosities for different compositions. The results were obtained using the modified Urbain viscosity model, whose accuracy has been validated in numerous previous studies. It can be seen that increasing the basicity and MgO content significantly decreases the slag viscosity, thereby improving slag fluidity during the smelting reduction of chromite. In contrast, increasing the Al_2O_3 content results in a higher slag viscosity, and the deterioration in fluidity hinders mass transfer. Figure 10d shows the liquidus temperatures and liquid fractions of slags with different compositions. Due to the presence of Cr_2O_3, the slags exhibit relatively high melting temperatures. As the basicity increases from 1.0 to 1.4, the liquidus temperature decreases

from 1640.87 °C to 1591.59 °C, which facilitates slag melting. In contrast, increasing the MgO and Al_2O_3 contents raises the liquidus temperature to 1623.73 °C and 1622.2 °C, respectively. Analysis of the liquid fraction indicates that increasing the basicity, MgO content, or Al_2O_3 content all reduce the liquid fraction of the slag, which is unfavorable for component mass transfer. Therefore, the influence of the chemical composition of slag on the smelting reduction efficiency is governed by multiple factors rather than a single physicochemical property.

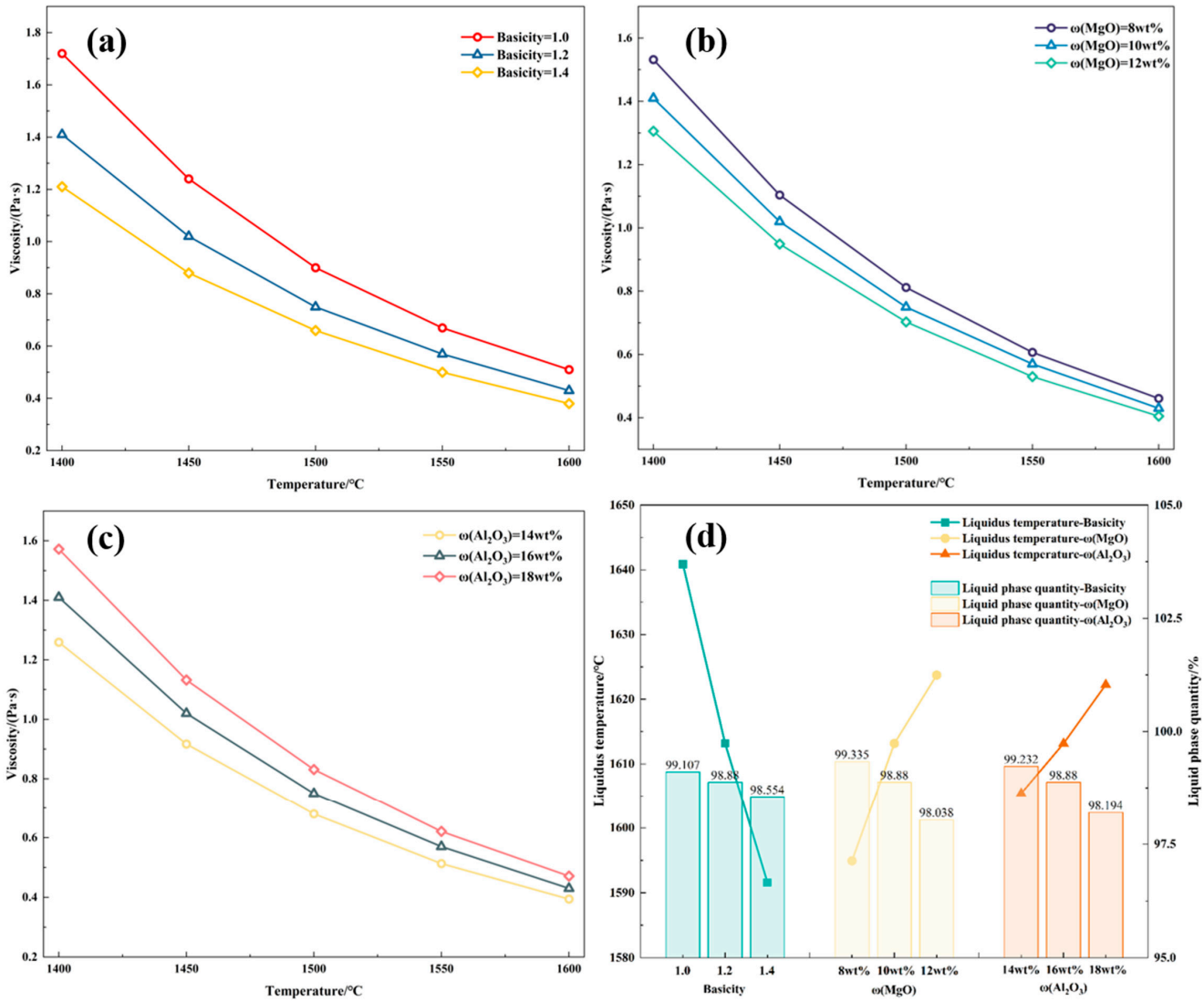


Figure 10. Viscosity and liquid-phase behavior of slag with varying compositions. (**a**) Viscosity at different basicity; (**b**) Viscosity at different MgO content; (**c**) Viscosity at different Al_2O_3 content; (**d**) Liquidus temperature and liquid phase quantity.

To further verify the influence of slag composition on the residual spinel phases in the reacted slag, the dissolution behavior of spinel under different basicity conditions is shown in Figure 11. At the reaction temperature of 1525 °C, the amounts of $MgCr_2O_4$ and $FeCr_2O_4$ gradually decrease with increasing basicity, indicating that higher basicity promotes the dissolution of chromite spinel and thereby accelerates the reduction reaction. However, when the temperature falls below 1400 °C during slag cooling, increasing the basicity to 1.4 promotes the re-precipitation of $FeCr_2O_4$, which is consistent with the SEM observations described above. Moreover, the amount of $MgAl_2O_4$ increases significantly with increasing basicity, which restricts the reduction of chromite spinel. The preceding

analysis also indicates that increasing basicity reduces the liquid phase fraction, promotes the formation of other solid phases (such as calcium silicates), and limits mass transfer. Therefore, the effect of alkalinity on chromite reduction is determined by the interplay between thermodynamic driving forces and kinetic limitations. This also explains the lower final chromium reduction degree obtained at a basicity of 1.4.

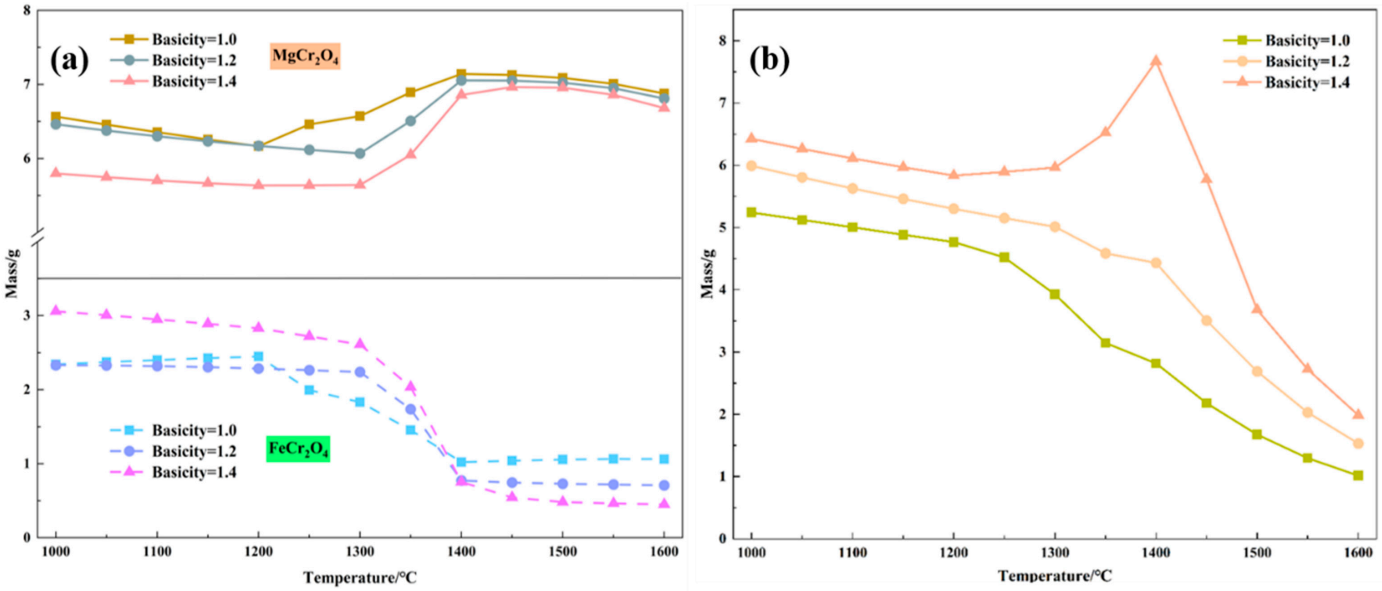


Figure 11. Effect of basicity on spinel equilibrium phase mass: (**a**) chromium spinel; (**b**) Mg-Al spinel.

As shown in Figure 12, increasing the MgO content decreases the amount of $FeCr_2O_4$ in the slag, which is gradually transformed into $MgCr_2O_4$, while the amount of $MgAl_2O_4$ increases markedly. These results indicate that the mass of $MgCr_2O_4$ and $MgAl_2O_4$ in the slag decreases with increasing MgO content. Although MgO is beneficial for improving slag fluidity, the excessive formation of solid-phase layers restricts the diffusion of Cr^{3+} within the chromite spinel. Consequently, after 60 min of reaction, the degree of reduction decreases with increasing MgO content.

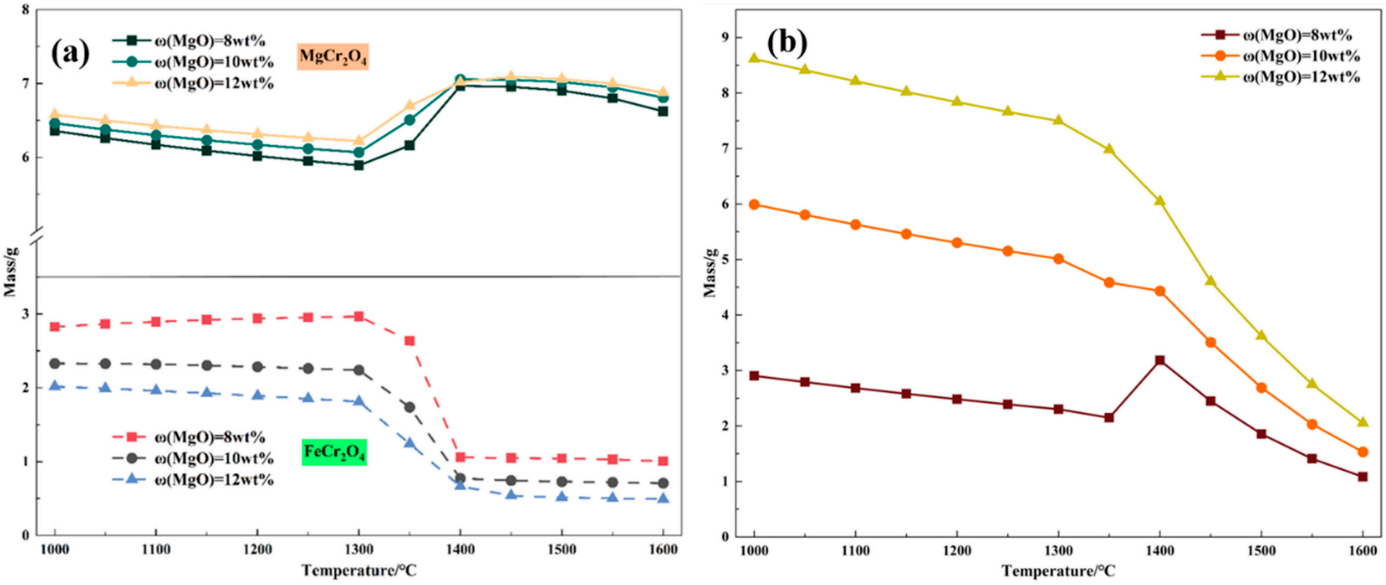


Figure 12. Effect of MgO content on spinel equilibrium phase mass: (**a**) chromite spinel; (**b**) Mg-Al spinel.

Figure 13 shows that as the Al_2O_3 content increases from 14 wt% to 16 wt%, the solubilities of both $MgCr_2O_4$ and $FeCr_2O_4$ increase, and the accelerated dissolution of chromite spinel significantly enhances the degree of reduction, which is consistent with the experimental observations discussed above. Meanwhile, the amount of $MgAl_2O_4$ also increases with increasing Al_2O_3 content, which impedes the reduction process during the later stage of the reaction and consequently lowers the chromium reduction degree.

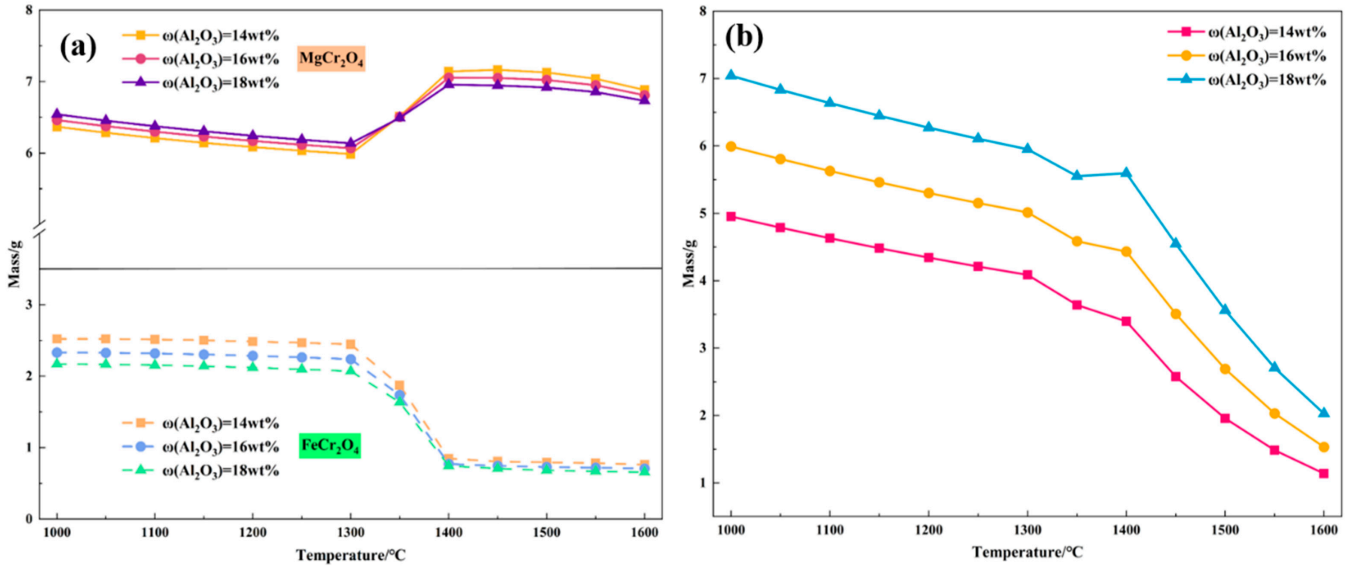


Figure 13. Effect of Al_2O_3 content on spinel equilibrium phase mass: (**a**) chromite spinel; (**b**) Mg-Al spinel.

4. Conclusions

The effects of slag composition on the smelting reduction behavior of chromite (using graphite as the reduction agent) were systematically investigated through smelting reduction experiments combined with microstructural characterization and thermodynamic analysis. The main conclusions are summarized as follows:

(1) The chemical composition of the slag significantly influences the smelting reduction behavior of chromite by regulating slag fluidity and interfacial mass transfer. Within the investigated composition range, the highest chromium reduction efficiency was obtained at a slag basicity of 1.2. However, when the basicity was further increased to 1.4, the final chromium reduction degree decreased.

(2) Increasing the MgO content improves slag fluidity and enhances the degree of reduction during the initial stage of the reaction. However, excessive MgO promotes the formation of a Mg-Al-rich spinel layer on the surface of chromite particles, which hinders the outward diffusion of Cr^{3+} and significantly reduces the degree of reduction during the diffusion-controlled stage.

(3) Reducing the Al_2O_3 content effectively decreases the slag viscosity and improves mass transfer, thereby promoting the reduction of chromite. When the Al_2O_3 content was 14 wt%, the highest chromium content in the hot metal was obtained. Furthermore, increasing the reaction temperature from 1525 °C to 1550 °C increased the chromium reduction degree to approximately 93%.

(4) SEM analysis revealed that the progressive dissolution of chromite spinel is accompanied by the apparent outward migration of Fe and Cr. As the reaction progresses, a Mg-Al-rich boundary layer forms around the unreacted core, which acts as a physical barrier that restricts the mass transfer and slows the reduction kinetics during the later stage.

Author Contributions: Conceptualization, J.Z. and Y.Z.; methodology, Y.Z., P.D. and Y.L.; validation, X.Z., M.L. and J.Y.; investigation, Y.Z.; resources, P.D. and Y.L.; data curation, Y.Z., X.Z., M.L. and J.Y.; writing—original draft preparation, Y.Z., X.Z., M.L. and J.Y.; writing—review and editing, J.Z. and Y.Z.; supervision, J.Z.; project administration, P.D. and Y.L. All authors have read and agreed to the published version of the manuscript.

Funding: This work was supported by National Natural Science Foundation of China (NSFC), Grant No. 52174296 and the Fundamental Research Funds for the Central Universities, Grant No. FRF-NP-20-06.

Data Availability Statement: The original contributions presented in this study are included in the article. Further inquiries can be directed to the corresponding author.

Acknowledgments: This work is supported by Key Laboratory of Metallurgical Industry Safety & Risk Prevention and Control, Ministry of Emergency Management.

Conflicts of Interest: Authors Ping Du and Yu Lu were employed by the Jiangsu Shagang Group Research Institute. The remaining authors declare that the research was conducted in the absence of any commercial or financial relationships that could be construed as a potential conflict of interest.

References

1. Simbi, D.J.; Tsomondo, M.B.C. Aspects of smelting reduction of chromite ore fines in CaO-FeO-Cr_2O_3-SiO_2-Al_2O_3 slag system by carbon dissolved in high carbon ferrochromium alloy bath. *Ironmak. Steelmak.* **2002**, *29*, 271–275. [CrossRef]
2. Tsomondo, M.; Simbi, D. Kinetics of chromite ore reduction from MgO-CaO-SiO_2-FeO-Cr_2O_3-Al_2O_3 slag system by carbon dissolved in high carbon ferrochromium alloy bath. *Ironmak. Steelmak.* **2002**, *29*, 22–28. [CrossRef]
3. Albertsson, G.J.; Teng, L.; Björkman, B. Effect of basicity on chromium partition in CaO–MgO–SiO_2–Cr_2O_3 synthetic slag at 1873 K. *Miner. Process. Extr. Metall.* **2014**, *123*, 116–122.
4. Li, Z.; Kato, C.; Kobayashi, Y. Determination of solubility of chromium oxide in the CaO–SiO_2–Cr_2O_3 slag system at 1873 K under moderately reducing conditions. *ISIJ Int.* **2021**, *61*, 2340–2344. [CrossRef]
5. Morita, K.; Inoue, A.; Takayama, N.; Sano, N. The Solubility of MgO-Cr_2O_3 in MgO-Al_2O_3-SiO_2-CaO Slag at 1600 °C under Reducing Conditions. *Tetsu-to-Hagane* **1988**, *74*, 999–1005. [CrossRef] [PubMed]
6. Ding, Y.L.; Merchant, A.J. Kinetics and mechanism of smelting reduction of fluxed chromite Part 1 Carbon–chromite–flux composite pellets in Fe–Cr–C–Si melts. *Ironmak. Steelmak.* **1999**, *26*, 247–253. [CrossRef]
7. Ding, Y.L.; Merchant, A.J. Kinetics and mechanism of smelting reduction of fluxed chromite Part 2 Chromite–flux pellets in Fe–C–Si melts. *Ironmak. Steelmak.* **1999**, *26*, 254–261. [CrossRef]
8. Xiao, Y.; Wei, K.; Wang, L.; Liu, S.; He, X.; Chou, K. Influence of Slag Chemistry on the Dissolution of $FeCr_2O_4$ in CaO–SiO_2–Al_2O_3–MgO Slag with Graphite Crucible. *ISIJ Int.* **2023**, *63*, 613–621.
9. Tangstad, M.; Bublik, S.; Haghdani, S.; Einarsrud, K.E.; Tang, K. Slag Properties in the Primary Production Process of Mn-Ferroalloys. *Metall. Mater. Trans. B* **2021**, *52*, 3688–3707. [CrossRef]
10. Seetharaman, S.; Mukai, K.; Sichen, D. Viscosities of slags-an overview. *Steel Res. Int.* **2005**, *76*, 267–278. [CrossRef]
11. Sohn, I.; Min, D.J. A review of the relationship between viscosity and the structure of calcium-silicate-based slags in ironmaking. *Steel Res. Int.* **2012**, *83*, 611–630. [CrossRef]
12. Zhang, Y.; Jiao, K.; Zhang, J.; Fan, X. Viscosity and Structural Characteristics of HIsmelt Chromium-Containing Slag. *Metall. Mater. Trans. B* **2025**, *56*, 1423–1433. [CrossRef]
13. Jakobsson, A.; Sichen, D.; Seetharaman, S.; Viswanathan, N. Interfacial phenomena in some slag-metal reactions. *Metall. Mater. Trans. B* **2000**, *31*, 973–980. [CrossRef]
14. Chen, X.; Wang, N.; Chen, M.; Yao, H. Influence of Al_2O_3 and Cr_2O_3 Content on Viscosity and Chromium Immobilization via Spinel Crystallization in High-alumina Slag Systems. *Ceram. Int.* **2025**, *51*, 50315–50323. [CrossRef]
15. Li, J.; Xu, A.; He, D.; Yang, Q.; Tian, N. Effect of FeO on the formation of spinel phases and chromium distribution in the CaO-SiO_2-MgO-Al_2O_3-Cr_2O_3 system. *Int. J. Miner. Metall. Mater.* **2013**, *20*, 253–258. [CrossRef]
16. Albertsson, G.; Teng, L.; Björkman, B.; Seetharaman, S.; Engström, F. Effect of low oxygen partial pressure on the chromium partition in CaO–MgO–SiO_2–Cr_2O_3–Al_2O_3 synthetic slag at elevated temperatures. *Steel Res. Int.* **2013**, *84*, 670–679. [CrossRef]
17. Wu, X.R.; Ma, B.; Lü, H.H.; Li, L.S.; Shen, X.M. Precipitation behaviour of chromium in CaO-MgO-SiO_2-Al_2O_3-Cr_2O_3-Fe_2O_3 slag system. *Adv. Mater. Res.* **2015**, *1073*, 21–27. [CrossRef]
18. Nakasuga, T.; Sun, H.; Nakashima, K.; Mori, K. Reduction rate of Cr_2O_3 in a solid powder state and in CaO–SiO_2–Al_2O_3–CaF_2 slags by Fe–C–Si melts. *ISIJ Int.* **2001**, *41*, 937–944. [CrossRef]

19. Demir, O.; Eric, R.H. Rate and mechanism of reduction-dissolution of chromite in liquid slags. *High Temp. Mater. Process.* **2013**, *32*, 255–263. [CrossRef]
20. Guo, Y.; Li, Z.; Liu, F.; Wang, S.; Chen, F.; Yang, L.; Li, Z. Corrosion behavior of CaO–Al_2O_3–SiO_2–MgO-Cr_2O_3 slag on MgO refractory brick for smelting of chromite. *J. Eur. Ceram. Soc.* **2024**, *44*, 544–556. [CrossRef]
21. Eissa, M.; El-Farmawy, H. Carbothermic smelting of high carbon ferrochromium alloy from low and high grade chromite ores. *Ironmak. Steelmak.* **2012**, *39*, 31–37. [CrossRef]
22. Xiao, Y.; Wang, L.; Liu, S.; He, X.; Chou, K.-C. Kinetic mechanism of $FeCr_2O_4$ reduction in carbon-containing iron melt. *J. Min. Metall. Sect. B Metall.* **2023**, *59*, 113–123. [CrossRef]
23. Zheng, H.; Zhou, S.; Zhang, S.; Li, Y.; Zhang, B.; Shen, F.; Wang, Z.; Han, T. Viscosity Estimation of TiO_2-Bearing Blast Furnace Slag with High Al_2O_3 at 1500 °C. *Metals* **2023**, *13*, 573. [CrossRef]
24. Forsbacka, L.; Holappa, L.; Kondratiev, A.; Jak, E. Experimental study and modelling of viscosity of chromium containing slags. *Steel Res. Int.* **2007**, *78*, 676–684. [CrossRef]
25. Xuan, W.; Guhl, S.; Zhang, Y.; Zhang, J.; Meyer, B. A structural viscosity model for silicate slag melts based on MD simulation. *Ceram. Int.* **2022**, *48*, 28291–28298. [CrossRef]
26. Uslu, E.; Eric, R. The reduction of chromite in liquid iron-chromium-carbon alloys. *J. S. Afr. Inst. Min. Metall.* **1991**, *91*, 397–409.
27. Soykan, O.; Eric, R.; King, R. The reduction mechanism of a natural chromite at 1416 °C. *Metall. Trans. B* **1991**, *22*, 53–63. [CrossRef]
28. Hazar-Yoruç, A. Reduction mechanism of chromite spinel with carbon. *Min. Metall. Explor.* **2007**, *24*, 115–120. [CrossRef]
29. Chakraborty, D.; Ranganathan, S.; Sinha, S. Investigations on the carbothermic reduction of chromite ores. *Metall. Mater. Trans. B* **2005**, *36*, 437–444. [CrossRef]

Disclaimer/Publisher's Note: The statements, opinions and data contained in all publications are solely those of the individual author(s) and contributor(s) and not of MDPI and/or the editor(s). MDPI and/or the editor(s) disclaim responsibility for any injury to people or property resulting from any ideas, methods, instructions or products referred to in the content.